SPARSE MULTIPATH MIMO CHANNELS: PERFORMANCE IMPLICATIONS BASED ON MEASUREMENT DATA

Michail Matthaiou[1]*, Akbar M. Sayeed*[2]*, and Josef A. Nossek*[1]

[1] Institute for Circuit Theory and Signal Processing, Technische Universität München (TUM), Arcistrasse 21, 80 333, Munich, Germany
email:{matthaiou,nossek}@nws.ei.tum.de
[2] Department of Electrical and Computer Engineering, University of Wisconsin-Madison, 3617 Engineering Hall, WI 53706, Madison, U.S.A.
email:akbar@engr.wisc.edu

ABSTRACT

The main focus of the present contribution is on the statistical assessment of Multiple-Input Multiple-Output (MIMO) systems from the viewpoint of underlying multipath sparsity. In contrast to the implicit assumption of rich multipath in the prevalent i.i.d. MIMO fading model, recent investigations and measurement campaigns have shown that physical channels exhibit a sparse multipath structure that in turn leads to spatial correlation. Using a set of measured data and a well-known analytical model, the measured MIMO channel matrix is decomposed in terms of fixed virtual transmit and receive angles, thereby providing a simple geometric interpretation of the scattering environment. It is demonstrated that the presence of direct or obstructed Line-of-Sight (LoS) components strongly correlates with channel sparsity; consequently, the number of spatial degrees of freedom (DoF) is severely limited compared to that in the i.i.d. model. In the sequel, we investigate the relationship between the channel sparsity structure and the mean of propagation paths and quantify the impact of channel sparsity on two key MIMO channel metrics: ergodic capacity and diversity level. In all cases, the analysis of measured data reveals an approximate concave quadratic variation in capacity, diversity and mean number of paths as a function of the number of DoF, thereby suggesting a fundamental inter-dependency between all these features.

1. INTRODUCTION

The rapid advances in the area of Multiple-Input Multiple-Output (MIMO) technology over the last years, have led to a renewed interest in MIMO channel modeling. Accurate channel modeling is critical for maximal exploitation of MIMO technology, both in terms of performance prediction and integration into real-time applications. In particular, it is widely recognized that the widely used i.i.d. fading MIMO channel model (see e.g., [1]), based on the implicit assumption of a rich multipath scattering environment, is an exception rather than the norm in practice. In fact, various stochastic modeling approaches have been proposed for capturing the joint spatial statistical characteristics between the transmitter (Tx) and receiver (Rx) (see for instance [2, 3, 4] and references therein).

A plethora of recent theoretical investigations [5, 6, 7] and MIMO measurement campaigns [4, 11] has shown that physical wireless channels exhibit a sparse multipath structure due to the lack of sufficient richness in the scattering environment. Formally, a *sparse MIMO channel* exhibits fewer spatial degrees of freedom (DoF) compared to the upper limit imposed by the number of antennas. The primary goal of this paper is to further investigate the fundamental dependencies between multipath sparsity and the key channel metrics: ergodic capacity and diversity level. This is accomplished using a set of indoor measured data whereas the necessary channel modeling framework is based on the Virtual Channel Representation (VCR) [3]. The data analysis reveals a strong dependence of channel sparsity on the nature of the multipath scattering environment. Furthermore, ergodic capacity, diversity level, and the mean number of propagation paths experience an approximate concave quadratic variation as a function of the DoF in the channel, thereby indicating a strong inter-connection between these features induced by multipath sparsity.

The paper is organized as follows: In Section 2, the theoretical background of the VCR model and multipath sparsity are discussed. Section 3 is devoted to the description of an indoor MIMO measurement campaign while Section 4 elaborates on the data analysis from different practical perspectives of interest. Finally, Section 5 concludes the paper.

A note on notation: We use upper and lower case boldfaces to denote matrices and vectors. Moreover, the symbols $(\cdot)^*$, $(\cdot)^T$, $(\cdot)^H$ correspond to complex conjugate, transposition and Hermitian transposition, respectively whereas $\odot$ returns the element-wise Schur-Hadamard multiplication. The vec$(\cdot)$ operator stacks the columns of a matrix into a vector while $\mathrm{tr}(\cdot)$, $\det(\cdot)$ and $\|\cdot\|_F$ will denote the trace, determinant and Frobenius norm of a matrix, respectively.

978-1-4244-3696-5/09/$25.00 © 2009 IEEE

2. VIRTUAL CHANNEL REPRESENTATION AND MULTIPATH SPARSITY

Let us consider a symmetric MIMO system equipped with N-element uniform linear arrays (ULAs) at bond ends. Assuming that all signal sources as well as the scatterers are located in the corresponding far field regions, the communication between the Tx and Rx can be effectively modeled as the superposition of L propagation paths. Then, the narrowband MIMO channel matrix $\mathbf{H} \in \mathbb{C}^{N\times N}$ reads as

$$\mathbf{H} = \sum_{\ell=1}^{L} \beta_\ell \boldsymbol{\alpha}_r(\theta_{r,\ell})\boldsymbol{\alpha}_t^H(\theta_{t,\ell}) \tag{1}$$

where the parameters $\{\theta_{r,\ell}\}$, $\{\theta_{t,\ell}\}$ and $\{\beta_\ell\}$ are the Angle-of-Arrival (AoA), Angle-of-Departure (AoD) and complex gain of the ℓ-th wave, while $\boldsymbol{\alpha}_r(\theta_{r,\ell})$ and $\boldsymbol{\alpha}_t(\theta_{t,\ell})$ denote the receive and transmit steering vectors, respectively. Although the above equation is often being used in the analysis of wireless propagation, it imposes a non-linear relationship between the channel matrix and the multipath parameters.

In light of this fact, the linear VCR model was developed which partitions the angular range into fixed, predefined directions which are determined by the spatial resolution of the system. The main idea behind VCR is that the finite number of antennas represent nonetheless a discrete sampling in the aperture domains which are directly related to the angular domains via a Fourier transform (FT). The use of FT explains why the model can be applied merely to ULA configurations as the sampling needs to be uniform in the aperture domains. The key equation of the model is given according to

$$\mathbf{H} = \sum_{m=1}^{N}\sum_{n=1}^{N} \mathbf{H}_v(m,n)\boldsymbol{\alpha}_r(\tilde{\theta}_{r,m})\boldsymbol{\alpha}_t^H(\tilde{\theta}_{t,n}) = \widetilde{\mathbf{A}}_r\mathbf{H}_v\widetilde{\mathbf{A}}_t^H \tag{2}$$

where $m,n = 1,\ldots,N$ and $\{\tilde{\theta}_{r,m} = m/N\}$, $\{\tilde{\theta}_{t,n} = n/N\}$ represent the virtual receive and transmit angles. The unitary matrices $\widetilde{\mathbf{A}}_r$ and $\widetilde{\mathbf{A}}_t$ are the channel independent discrete Fourier transform (DFT) matrices of size $(N \times N)$. The columns of these orthonormal matrices constitute steering vectors into the directions of virtual angles. It can be easily inferred that $\mathbf{H}$ and $\mathbf{H}_v$ are inherently related via a unitary transformation, i.e. $\mathbf{H}_v = \widetilde{\mathbf{A}}_r^H\mathbf{H}\widetilde{\mathbf{A}}_t$.

A critical characteristic of the VCR framework, is the *virtual channel power matrix*, $\boldsymbol{\Omega}_v(m,n) = E\left[|\mathbf{H}_v(m,n)|^2\right]$, whose positive and real valued coefficients $\omega_v(m,n)$ specify the mean amount of energy coupled from the n-th transmit virtual angle to the m-th receive virtual angle. The structure of $\boldsymbol{\Omega}_v$ is heavily dependent on the spatial arrangement of scatterers and determines all the fundamental features of a MIMO channel, i.e. number of multiplexed data streams, degree of diversity and beamforming gain. This is attributed to the virtual path partitioning which approximately makes the virtual coefficient statistically independent and that is why $\boldsymbol{\Omega}_v$ is able to capture the channel statistics. According to [5], the number of independent DoF, D, in a MIMO channel is equal to the number of entries in $\mathbf{H}_v$ with non-vanishing power, or

$$D = |\{(m,n) : \boldsymbol{\Omega}_v(m,n) > 0\}|. \tag{3}$$

Likewise, a $N \times N$ MIMO channel is called *sparse* as long as it contains $D < N^2$ non-vanishing coefficients. In reality, it has been shown that dominant virtual coefficients tend to be sparse, since for practical wireless channels the majority of DoF are either zero or nearly zero [4, 5, 6].

3. INDOOR MIMO MEASUREMENTS

An indoor measurement campaign was carried out in Vienna University of Technology in an area with many office partitions (see Fig. 1). The measurements were conducted at a carrier frequency of 5.2 GHz and an operation bandwidth of 120 MHz while the channel sounder was probed at 193 equispaced frequency bins covering the overall bandwidth [8].

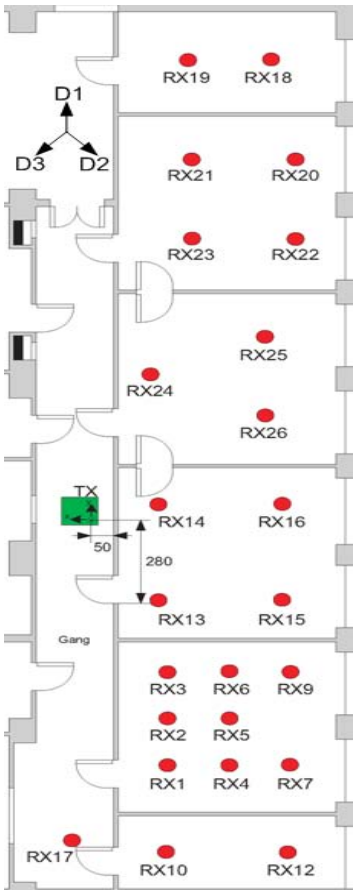

Fig. 1. Layout of the measurement environment.

The Rx employed a ULA of eight vertically-polarized elements with an inter-element distance of 0.4λ which was fully

calibrated, using the method described in [9], in order to remove the undesired effects of mutual coupling, non-identical element response and other array imperfections. At the Tx, an omni-directional sleeve antenna was moved on a (10×20) rectangular grid with element spacings of 0.5λ, forming a virtual Tx matrix with no mutual coupling. By considering a virtual eight-element ULA on each row, a total number of $13\times10=130$ spatial realizations of the 8×8 MIMO transfer matrix is acquired. Hence, a total set of $130\times193=25,090$ space and frequency realizations per measurement scenario was obtained. For the following study, 24 different Rx locations were investigated in several offices while the Tx was positioned at a fixed position in the hallway. In order to capture the whole azimuth domain activity, the Rx was steered to three different broadside directions (spaced by 120°), thereby generating 72 data sets, i.e. combinations of Rx positions and directions. Hereafter, each data set will be denoted via the Rx location and broadside direction, e.g. 2D3.

4. DATA ANALYSIS

The first step of post-processing analysis includes the computation of the full spatial correlation matrix, which describes the joint correlation properties of both link ends, using all space and frequency realizations, as follows [2]

$$\mathbf{R_H} \triangleq E_{\mathbf{H}}\left[\mathrm{vec}\left(\mathbf{H}\right)\mathrm{vec}(\mathbf{H})^H\right]. \quad (4)$$

An estimate of the coupling matrix $\mathbf{\Omega}_v$ of the VCR model is also obtained via the measured channel matrix $\mathbf{H}$ as [3, 4]

$$\mathbf{\Omega}_v = E_{\mathbf{H}}\left[\left(\widetilde{\mathbf{A}}_r^H\mathbf{H}\widetilde{\mathbf{A}}_t^*\right)\odot\left(\widetilde{\mathbf{A}}_r^T\mathbf{H}^*\widetilde{\mathbf{A}}_t\right)\right]. \quad (5)$$

At a next step, the actual DoF at each measurement scenario are computed from the entries of $\mathbf{\Omega}_v$ after replacing the zero threshold in (3) with a more practical pseudo-noise level. We have herein considered as non-zero contributions all entries whose power falls above 10% of the maximum power entry

$$D = |\{(m,n) : \mathbf{\Omega}_v(m,n) \geq 0.1\max(\mathbf{\Omega}_v)\}|. \quad (6)$$

This threshold is well within the measured Signal-to-Noise ratio (SNR) and thus guarantees that the majority of the dominant components is identified [10]. At each measurement scenario, the mean number of paths L lying above the noise floor was also determined, using the super-resolution Space-Alternating Generalized Expectation Maximization (SAGE) algorithm (i.e. model order estimation problem)[1].

4.1. DoF and propagation environment classification

In this section, the number of DoF is estimated under different propagation conditions. Due to space constraints, we merely consider some indicative cases of Line-of-Sight (LoS), non-LoS (NLoS) and obstructed LoS (OLoS) propagation (c.f. Table 1). It can be easily seen that the LoS and OLoS locations (indicated by 'L' and 'O' respectively) exhibit a strong multipath sparsity, as the dominant paths mask the scattered waves making them lie under the noise floor and hence not contributing to the number of DoF. On the other hand, the NLoS Rx locations in the vicinity of the outer wall (illustrated by 'N') yield a larger number of DoF as a result of the weak high-order waves which bounce multiply off the surrounding walls. We can thus conclude that when a direct or obstructed LoS component is present in the communication link, the structure of the power coupling matrix is remarkably sparse.

Table 1. DoF at different Rx locations and orientations.

Rx loc.	DoF	Rx loc.	DoF	Rx loc.	DoF
9D1 (N)	35	13D1 (O)	2	14D1 (O)	5
14D3 (O)	4	16D1 (O)	6	16D3 (O)	6
18D2 (O)	8	19D3 (O)	6	24D3 (O)	7
20D1 (N)	42	22D2 (N)	51	25D1 (N)	26
25D2 (N)	54	26D1 (N)	43	26D2 (N)	33
17D1 (L)	8	17D2 (L)	5	17D3 (L)	3

A contour plot of the entries of $\mathbf{\Omega}_v$ at a representative OLoS location (13D1) is shown in Fig. 2. The plot shows an extremely sparse channel with only two dominant non-vanishing entries, representing the coupling between the associated transmit/receive virtual angles.

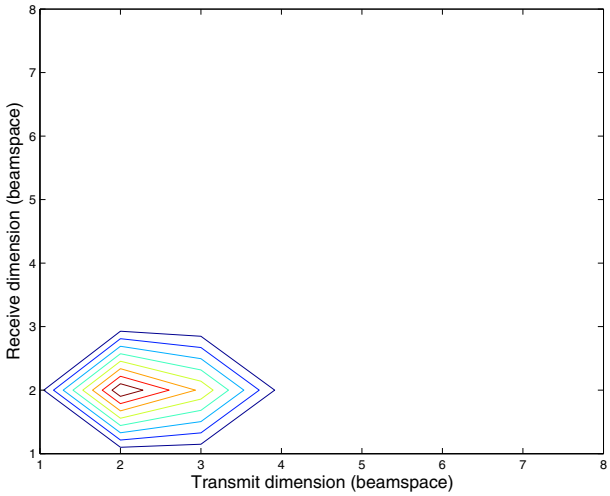

Fig. 2. Contour plot of $\mathbf{\Omega}_v$ for an extremely sparse measurement scenario (13D1, $D=2$).

It is also worth highlighting that the narrowband $\mathbf{\Omega}_v$ exhibits a larger angular spread than the wideband $\mathbf{\Omega}_v$ whose structure was investigated in the joint delay-angular domain in [11]. This implies that the dominant entries in the lat-

[1] A further discussion on the implementation of the SAGE algorithm is beyond the scope of the paper and the interested readers are referred to [10] and references therein for an additional insight.

ter case, conditioned on a particular resolvable delay, have a sparser distribution that those in the former.

4.2. Ergodic capacity

In order to assess the dependency between multipath sparsity and MIMO ergodic capacity, we assume that the Rx has perfect channel state information (CSI) while the Tx knows neither the statistics nor the instantaneous CSI. Then, a sensible choice for the Tx is to split the total amount of power equally among all data streams and the ergodic MIMO capacity (in bits/s/Hz) is given by the following well-known formula [1]

$$\overline{C} \quad = \quad E_{\mathbf{H}}\left[\log_2\left(\det\left(\mathbf{I}_N + \frac{\rho}{N}\mathbf{H}\mathbf{H}^H\right)\right)\right] \qquad (7)$$

where ρ denotes the SNR per receiver branch. Note that prior to the computation of ergodic capacity, the measured channel matrix is normalized so that

$$E\left[\|\mathbf{H}\|_F^2\right] = N^2. \qquad (8)$$

From a physical viewpoint, the path-loss effects are removed and the system is assumed to have perfect power control. In Fig. 3, the ergodic capacity is plotted against the number of spatial DoF at all measurement scenarios, for $\rho = 20$ dB.

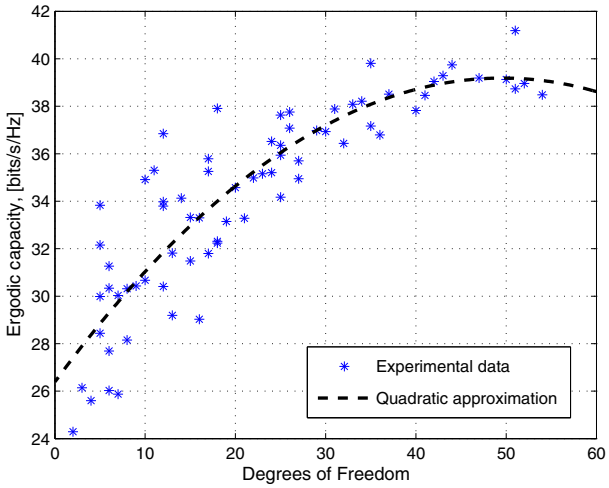

Fig. 3. Ergodic capacity, $\overline{C}$, against the spatial DoF, D ($\rho =$ 20 dB).

This graph indicates that $\overline{C}$ increases with the number of spatial DoF or as the scattering environment gets richer. The quadratic trend is an implication of the power allocation since for high D, the entries of $\mathbf{\Omega}_v$ are not all uniform and, consequently, the power in weaker dimensions is wasted. More importantly, it was found that apart from D, a critical factor affecting MIMO capacity is the spread of the non-vanishing entries of $\mathbf{\Omega}_v$. Generally speaking, a smooth $\mathbf{\Omega}_v$ delivers high capacities for large ρ, whereas for sparse channels a portion of power is inevitably wasted on the weaker entries whose contribution to the channel throughput is diminishing with increasing ρ. On the other hand, at low ρ, a peaky angular spectrum tends to become optimal as long as all power is allocated to the dominant virtual beam regardless of the actual number of non-vanishing entries. Similar conclusions were drawn at the vast majority of the considered scenarios and are consistent with [5, 7, 11]. It is also noteworthy that the distribution of D values in Table 1 evidently validates the presence of multipath sparsity since we notice a significant portion of them is well below the upper bound of $D_{max} = N^2 = 64$.

4.3. Diversity level

We next explore the impact of multipath sparsity on channel diversity which affects the reliability of communication; e.g, the slope of the error probability and outage capacity curves. In order to quantify the level of diversity, we use the notion of *diversity measure* that can effectively characterize equivalence classes of MIMO channels with similar performance in terms of ergodic/outage capacity and throughput [12]

$$\Psi(\mathbf{R}_{\mathbf{H}}) = \left(\frac{\mathrm{tr}(\mathbf{R}_{\mathbf{H}})}{\|\mathbf{R}_{\mathbf{H}}\|_F}\right)^2. \qquad (9)$$

One member of the equivalence class suffices to represent the whole class; thus, it can serve as our reference measure hereafter to disclose the inter-dependency between diversity and multipath sparsity. In Fig. 4 and 5, the diversity measure and mean number of paths are respectively depicted against the DoF, for all the 72 scenarios. In both cases, a quadratic regression curve is also overlaid which offers a rather good fit with the raw data, especially between L and D.

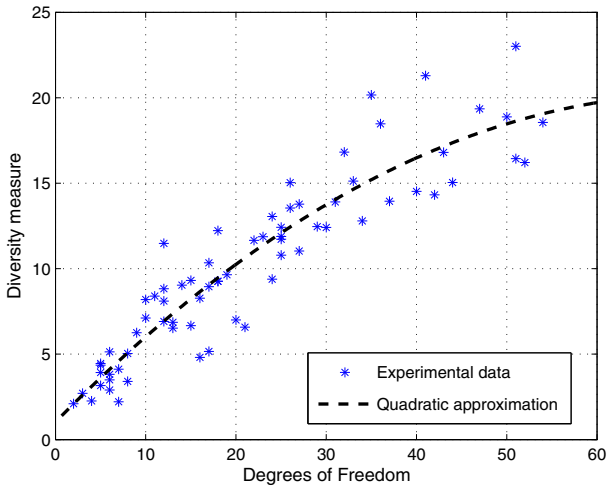

Fig. 4. Diversity measure, $\Psi(\mathbf{R}_{\mathbf{H}})$, of the measured data set against the spatial DoF, D.

More specifically, the diversity level is systematically enhanced by the presence of a larger number of non-vanishing

power entries in the coupling matrix. This phenomenon is expected since the amount of diversity associated with each MIMO channel is a function of the number of virtual receive angles that couple with each virtual transmit angle, and vice versa [3, 5, 6]. Please note that a similar quadratic trend was observed between L and $\Psi(\mathbf{R_H})$ as well, thereby verifying the well established view that a large number of (resolvable) multipath components favors channel diversity. Likewise, we recall that the DoF ultimately depend on the number of resolvable paths that lie in the intersection of the virtual spatial beams; in fact, the entries of $\mathbf{\Omega}_v$ can be very well approximated by the sum of powers of the corresponding paths.

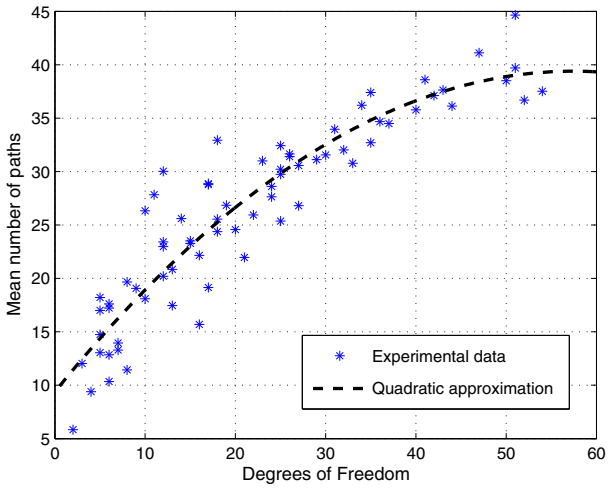

Fig. 5. Mean number of paths, L, against the spatial DoF, D.

5. CONCLUSION

In this paper, we investigated the notion of multipath sparsity and its impact on MIMO system performance using a set of indoor measured data. It was clearly shown that the physical nature of the scattering environment has a noticeable impact on the DoF afforded by a MIMO channel since it determines the number of non-vanishing entries and the angular spread of the joint power spectrum. The relationship between sparsity (number of DoF) and the key MIMO metrics of ergodic capacity and diversity level were also investigated. An approximate quadratic fit seems to exist between ergodic capacity/diversity level and the DoF and, similarly, between the DoF and number of dominant multipath propagation paths, thereby revealing a strong dependency between these metrics.

6. ACKNOWLEDGMENTS

The authors would like to thank Dr. John Thompson from University of Edinburgh, U.K. and Dr. Markus Herdin, formerly of Vienna University of Technology, for providing them with access to the measurement data discussed in this paper.

7. REFERENCES

[1] I. E. Telatar, "Capacity of multi-antenna Gaussian channels," *ATT-Bell Labs Internal Tech. Mem.*, June 1995.

[2] J. P. Kermoal, L. Schumacher, K. I. Pedersen, P. E. Mogensen, and F. Frederiksen, "A stochastic MIMO radio channel model with experimental validation," *IEEE J. Selec. Areas Commun.*, vol. 20, pp. 1211–1226, Aug. 2002.

[3] A. M. Sayeed, "Deconstructing multi-antenna fading channels," *IEEE Trans. Sig. Proc.*, vol. 50, no. 10, pp. 2563–2579, Oct. 2002.

[4] W. Weichselberger, M. Herdin, H. Özcelik, and E. Bonek, "A stochastic MIMO channel model with joint correlation of both link ends," *IEEE Trans. Wirel. Commun.*, vol. 5, no. 1, pp. 90–100, Jan. 2006.

[5] A. M. Sayeed and V. Raghavan, "Maximizing MIMO capacity in sparse multipath with reconfigurable antenna arrays," *IEEE J. Special Topics in Sig. Proc.*, vol. 1, no. 1, pp. 156–166, June 2007.

[6] V. Raghavan, G. Hariharan, and A. M. Sayeed, "Capacity of sparse multipath channels in the ultrawideband regime," *IEEE J. Special Topics in Sig. Proc.*, vol. 1, no. 3, pp. 357–371, Oct. 2007.

[7] A. M. Sayeed, V. Raghavan, and J. Kotecha, "Capacity of space-time wireless channels: A physical perspective," in *Proc. Inform. Theory Work. (ITW)*, San Antonio, TX, Oct. 2004, pp. 434–439.

[8] M. Herdin, H. Özcelik, H. Hofstetter, and E. Bonek, "Variation of measured indoor MIMO capacity with receive direction and position at 5.2 GHz," *IEE Elect. Lett.*, vol. 38, no. 21, pp. 1283–1285, Oct. 2002.

[9] K. Pensel and J. A. Nossek, "Uplink and downlink calibration of an antenna array in a mobile communication system," *COST 259 Tech. Doc.*, In *TD(97)55*, Lisbon, Portugal, Sept. 1997.

[10] M. Matthaiou, D. I. Laurenson, and J. S. Thompson, "Detailed characterisation of an indoor MIMO channel in the double directional spatial domain," *IET Microw., Anten. & Propag.*, vol. 3, no. 2, pp. 205–213, Mar. 2009.

[11] Z. Yan, M. Herdin, A. M. Sayeed, and E. Bonek, "Experimental study of MIMO channel statistics and capacity via the virtual channel representation," *Tech. Rep.*, Univ. Winsconsin-Madison, Feb. 2007, available `http://dune.ece.wisc.edu/pdfs/zhou_meas.pdf`.

[12] M. T. Ivrlač and J. A. Nossek, "Quantifying diversity and correlation in Rayleigh fading MIMO communication systems," in *Proc. Intern. Symp. Sig. Proc. Inf. Techn. (ISSPIT)*, Darmstadt, Germany, Dec. 2003, pp. 158–161.